Journal of Colloid and Interface Science 608 (2022) 1449–1456

Contents lists available at ScienceDirect

Journal of Colloid and Interface Science

journal homepage: www.elsevier.com/locate/jcis

Fabrication of electron–acceptor staggered AB Covalent triazine-based frameworks for enhanced visible-light-driven H_2 evolution

Yinyin Li [a], Rui Zhang [a], Cuiyan Li [b], Hui Li [b,*], Qianrong Fang [b,*], Tengfeng Xie [a,*]

[a] Institute of Physical Chemistry, College of Chemistry, Jilin University, Changchun 130012, PR China
[b] State Key Laboratory of Inorganic Synthesis and Preparative Chemistry, College of Chemistry, Jilin University, Changchun 130012, PR China

GRAPHICAL ABSTRACT

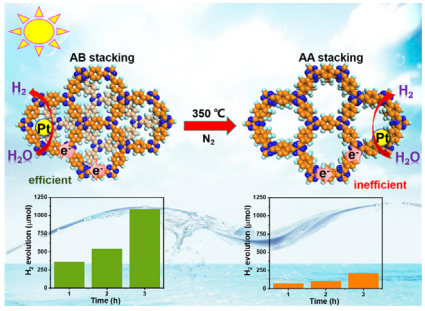

ARTICLE INFO

Article history:
Received 20 August 2021
Revised 6 October 2021
Accepted 18 October 2021
Available online 20 October 2021

Keywords:
Covalent triazine-based frameworks
AB stacking
Charge separation
H_2 evolution
Photocatalyst

ABSTRACT

Covalent triazine-based frameworks (CTFs) have been emerged as a promising organic material for photocatalytic water splitting. However, all of the CTFs only are in the form of AA stacking model to participate in water splitting. Herein, two CTF-1 isomers with different stacking models (eclipsed AA, staggered AB) were obtained by modulating the reaction temperature. Interestingly, experimental and theoretical calculations showed that the crystalline AB stacking CTF-1 possessed a much higher activity for photochemical hydrogen evolution (362 μmol g^{-1} h^{-1}) than AA stacking CTF-1 (70 μmol h^{-1} g^{-1}) for the first time. The outstanding photochemical performance could be attributed to its distinct structural feature that allows more N atoms with higher electron-withdrawing property to be involved in the water reduction reaction. Notably, as a cathode material for PEC water reduction, AB stacking CTF-1 also demonstrated an excellent saturated photocurrent density up to 77 μA cm^{-2} at 0 V vs. RHE, which was superior to the AA stacking CTF-1 (47 μA cm^{-2}). Furthermore, the correlation between stacking models and photocatalytic H_2 evolution of CTF-1 were investigated. This study thus paves the path for designing optimal photocatalyst and extending the novel applications of CTF-based materials.

1. Introduction

Solar-to-hydrogen (H_2) conversion has been considered as an attractive and sustainable technique to solve the global energy crisis [1]. Since TiO_2 was first reported as an effective photoelectrode for photoelectrochemical (PEC) water splitting by Fujishima et al. [2], a series of semiconductor materials have been studied for photocatalysis [3,4]. Among them, organic semiconductors have arisen as promising materials for photocatalytic production of hydrogen to solve the energy crisis [5–8]. Highly efficient solar-driven H_2 evolution could be achieved through these efficient photocatalysts with enhanced light harvesting and facilitated

* Corresponding authors.
E-mail addresses: postlh@jlu.edu.cn (H. Li), qrfang@jlu.edu.cn (Q. Fang), xietf@jlu.edu.cn (T. Xie).

https://doi.org/10.1016/j.jcis.2021.10.100
0021-9797/

carrier mobility can be synthesized based on the deliberation that was acquired by rational design and synthesis of photocatalysts [9–13]. Wang et al. have performed a pioneering work to use graphitic carbon nitride (g-C_3N_4) as one promising organic material for efficient H_2 evolution from water with Pt cocatalyst in the presence of a sacrificial electron donor (SED) [14]. Since then, a series of semiconductors involving organic polymers have been explored to improve the efficiency of photocatalytic hydrogen evolution, such as metal–organic frameworks (MOFs) [7,15,16], covalent triazine-based frameworks (CTFs) [17–19] or covalent organic frameworks (COFs) [20–22]. The light-harvesting ability related to band gaps could be controlled on organic photocatalysts due to considerable functionalities and diverse synthetic designs. Metal-free conjugated polymers as one of intriguing functional organic materials exhibited a great photocatalytic activity for water splitting.

With abundant nitrogen, modular geometry and tuned electronic structures, CTFs as promising alternatives to inorganic semiconductors have been applied to photocatalysis for, such as photoreduction of CO_2, photocatalytic conversion of chemical molecules, photocatalytic water splitting, and photodegradation of organic pollutants etc [23–25]. CTFs exhibited great potential for the photocatalytic H_2 evolution through water splitting [19,26,27]. For CFTs, different stacking between layers would result in the interlayer coupling of either C—C or C—N bonds, which could affect the photocatalytic activity for hydrogen evolution [28]. Only a small number of AA stacking CTFs have been explored for their photocatalysis of hydrogen evolution, since the conjugated structures and semiconductor characteristics were easily destroyed during the carbonization of CTFs under harsh synthetic conditions [29]. Compared with AA stacking, AB stacking presents more active sites involved in charge transfer and separation. However, the majority of CTFs exist in the form of AA stacking model [30], and the photocatalytic activity for H_2 evolution over AB stacking CTFs has not been experimentally investigated.

In this work, we designed and synthesized CTF-1 with highly crystalline AA and AB stacking under mild and solvent-free conditions to elucidate the crucial relationship between stacking models and photocatalytic H_2 evolution. The AB stacking CTF-1 showed an outstanding photochemical performance because of more N atoms with higher electron-withdrawing feature in the structure. The AB stacking CTF-1 with more active sites enabled sustained H_2 evolution with an excellent rate (362 μmol h^{-1} g^{-1}) than AA stacking CTF-1 (70 μmol h^{-1} g^{-1}) in the presence of triethanolamine (TEOA) as the SED in water under visible light (≥395 nm). Moreover, the behaviour of photoelectron was proved by photophysical methods and theoretical calculations. It was indicated that the donor–acceptor active sites of AB stacking could promote the separation of photogenerated carriers. Therefore, as the cathode material for PEC water reduction, AB stacking CTF-1 demonstrated an excellent saturated photocurrent density up to 77 μA cm^{-2} at 0 V vs. RHE, superior to the AA stacking CTF-1 (47 μA cm^{-2}). The correlation between stacking models and photocatalytic H_2 evolution of CTF-1 was discussed in detail. The present study facilitates the developing efficient photocatalyst and practical applications of CTFs.

2. Experimental section

2.1. Materials

1,4-dicyanobenzene (DCB), 1,4-dicyanotetrafluorobenzene (DCTF-1B) and superacids including trifluoroacetic acid (CF_3COOH), methanesulfonic acid (CH_3SO_3H), trifluoromethanesulfonic acid (CF_3SO_3H), fluorosulfonic acid (FSO_3H) and fluoroantimonic acid ($HSbF_6$) were purchased from commercial sources. (The reagents were used without further purification, unless indicated otherwise).

2.2. Synthesis of CTF-1 materials

In this work, the CTF-1 including AB stacking and AA stacking aromatic triazine linkages were synthesized via covalent linking, which was analogous to the method reported previously [31]. Synthesis of AB stacking CTF-1: 1,4-dicyanobenzene (DCB) (2 mmol, 0.256 g) and CF_3SO_3H (1 mmol, 0.15 g) were mixed into a Pyrex tube and degassed with nitrogen for 15 min, and then the mixture was cooled down in liquid nitrogen. Subsequently, the tube was heated to 250 °C in an oven with ramping rate of 5 °C min^{-1} and held at that temperature for 12 h. After that, the Pyrex tube was cooled down to room temperature and then immersed in liquid nitrogen for several minutes when the reaction was finished. The solid was collected and washed three times with water and acetone. After drying at 60 °C under vacuum for 12 h, the AB stacking CTF-1 was obtained as orange powder.

2.3. Characterizations

The X-ray diffraction (XRD) was performed by using a Rigaku/Ultima IV diffraction instrument with Cu Ka radiation (k = 1.5418 Å, 50 kV, 200 mA) and the range of 2 θ was from 5° to 40° to analyse the crystal structure. The scanning electron microscopy (SEM) was conducted on a Hitachi FE-SEM S4800 to observe the surface morphology of the samples. Transmission electron microscopy (TEM) image was obtained on FEI Tecnai G2 F20 transmission electron microscopy. The FTIR spectra (KBr) were obtained using a SHIMADZU IRAffinity-1 Fourier transform infrared spectrophotometer. The UV–vis diffuse reflectance spectra in the range of 300–800 nm was measured by a UV–VIS-NIR spectrophotometer (Shimadzu UV-3600) using $BaSO_4$ as background. X-ray photoelectron spectroscopy (XPS) was tested on a Thermo VG Scientific Escalab 250 spectrometer with a monochromated AlKa excitation source. Thermogravimetric analysis (TGA) was recorded on a SHIMADZU DTG-60 thermal analyzer under N2. Adsorption isotherms of N_2 at 77 K were measured to estimate pore size distributions for AA stacking and AB stacking. Surface photovoltage (SPV) was used to investigate the photogenerated carrier behaviour of the sample on a home-made equipment [32]. The equipment for SPV was assembled with a 500 W xenon lamp (CHF-XM-500 W, GLOBAL Xenon Lamp), a monochromator (ZLolix SBP500), a lock-in amplifier (SB830-DSP) with a light chopper (SR540) and a computer. The testing frequency was set as 24 Hz and the wavelength range was from 300 to 800 nm. The sample was assembled to "FTO-mica-sample-FTO" configuration (detailed preparation method shown in Supporting Information). The home-made equipment for transient photovoltage (TPV) included a laser pulse (Polaris II, New Wave Research, Inc) and a 500 MHz digital phosphor oscilloscope (TDS 5054, Tektronix).

To further confirm the charge transfer of AA and AB stacking CTF-1, the SPV and TPV measurements were carried out. The SPV measurement was performed based on the lock-in amplifier. And the SPV spectra in our experiments were measured as the in-phase signals (Uxsignal). The measurement system consisted of a source of monochromatic light, a lock-in amplifier (SR830, Stanford Research Systems, Inc.) with a light chopper (SR540, Stanford Research Systems, Inc.), and a sample chamber. The monochromatic light was provided by a 500 W xenon lamp equipped with a monochromator (SBP500, Zolix) that was chopped at a frequency of 23 Hz. All the measurements were operated at room temperature and under ambient pressure [32].

The TPV measurement was implemented on a home-made system to investigate the separation and behavior of photogenerated

charge carriers. In short, the testing system was composed of a third-harmonic Nd:YAG laser (Q-smart 450, Quantel), a 500 MHz digital phosphor oscilloscope (TDS 5054, Tektronix) and a photovoltage cell. It was noted that the wavelength and intensity of the laser pulse were 355 nm and 100 μJ respectively.

Electron spin resonance (ESR) of AA and AB stacking CTF-1 was conducted at room temperature and the g value was calculated using the expression as follows:

$$g = h\mu/H\beta$$

where, h (Planck's Constant) = 6.6262 × 10^{-34} J·s; β (Bohr Magneton) = 9.2741 × 10^{-28} J/mT; μ = micro frequency × 10^{6} [microwave frequency = 9443.725 MHz (used for measuring)].

2.4. Electrochemical measurement

A CHI660D electrochemical workstation (Chenhua Instruments Co., Shanghai) was employed to measure Mott-Schottky (M−S) plot and chopped photocurrent density-time (j–t) curve. A 300 W xenon lamp (PLS-SXE300, Beijing Perfect Light, China) was used as the light source. In a typical electrochemical test, Na_2SO_4 aqueous solution (0.5 M) served as the electrolyte in the standard three-electrode system with the sample (working electrode), Ag/AgCl (in saturated KCl, reference electrode), and Pt wire (counter electrode) [33]. The working electrode was fabricated as follows: 6 mg of as-synthesized sample and 6 μL of 10% Nafion (DuPont) were uniformly dispersed in 600 μL of isopropanol solution. Subsequently, the mixture was treated under ultrasonication for 20 min to get the homogeneous suspension. And then, 10 μL of suspension was dropped on F-doped SnO_2-coated glass (FTO glass). After the natural drying under room temperature, the working electrode was obtained.

Based on the Nernst equation, the applied potential could be converted to the reversible hydrogen electrode (RHE):

$$E_{RHE} = E_{Ag/AgCl} + 0.059pH + E^{\theta}_{Ag/AgCl}$$

The linear sweep voltammetry (LSV) could be used to record the current vs potential curve.

The EIS was tested at 0 V vs. RHE under light irradiation (100 mW/cm^2) and with a frequency range of 10^5 Hz to 0.05 Hz.

2.5. Photocatalytic performance evaluation

H_2 evolution experiments were conducted under irradiation of 300 W xenon lamp with a cut-off filter of 395 nm. Triethanolamine (TEOA) was chosen as an optimized sacrificial agent to capture the photogenerated holes of the photocatalyst. A suspension of photocatalyst (10 mg) was added to 100 ml of triethanolamine (10 vol%) aqueous solution, followed by 20 min of sonication treatment. Finally, the suspended solution containing appropriate amounts of H_2PtCl_6 was bubbled with N_2 for 30 min. The mixture was irradiated under a 300 W xenon lamp in a quartz reactor at a constant temperature with circulating water. In this experiment, the H_2 production was tested on a GC-2014 gas chromatograph system (SHMADAZU) equipped with a thermal conductive detector and a 5A molecular sieve column, using nitrogen as the carrier gas. During the photocatalytic testing, each photocatalytic H_2 production reaction has been carried out at least 3 times to give the average value of H_2 production rate [34].

3. Results and discussion

3.1. Structural and chemical properties

The synthesis of AA and AB stacking CTF-1 was realized through a tandem transformation approach and highly crystalline CTF-1 were fabricated under mild conditions (Scheme 1). The powder X-ray diffraction (PXRD) analysis was performed to elucidate the structural features of the as-synthesized CTF-1. The peak at 7.12° from AA stacking CTF-1 is assigned to the in-plane reflection (100) (Fig. 1a). Three additional Bragg peaks at 12.35°, 14.25°, and 19.01° are attributed to the (110), (200), and (210) reflections. Compared with the AA stacking, For AB stacking, peak at 7.01° is ascribed to the in-plane reflection (100) and another peak at 18.8° corresponds to the (201) reflection in Fig. 1b. The refinement results matched well with the observed ones with a negligible difference and good agreement factors of AB stacking (Rp = 3.28% and Rwp = 2.50%) and AA stacking (*R*p = 2.97% and *R*wp = 2.31%). And the structure of as-synthesized sample was confirmed by powder X-ray diffraction (PXRD) analysis (Fig. S1-2). Geometry optimizations of the structural models were conducted using the Materials Studio software package. The simulated results agreed well with the experimental PXRD patterns from AA and AB stacking models, respectively. Moreover, the data shows that the structure of CTF has not changed after illumination in Fig.S3. The permanent porosities of AA stacking and AB stacking CTF-1 were assessed by nitrogen adsorption–desorption isotherm at 77 K in this work. The values of Brunauer–Emmett–Teller (BET) for the AA and AB stacking CTF-1 were calculated to be 520 and 236 m^2g^{-1} (Fig. 1c-d), respectively. Pore size distribution curves were shown in Fig. S4. These results indicated that AA stacking CTF-1 possessed a larger specific surface area than AB stacking CTF-1.

The detailed elemental composition of CTF-1 was analyzed by X-ray photoelectron spectroscopy (XPS) [31,35]. The survey curves demonstrate that C, N, O and F presented in AB stacking, whereas almost no F element existed in AA stacking CTF-1 (Fig. 2a). In the C 1s high-resolution XPS curves of the two materials (Fig. 2b), two strong peaks with binding energy of 284.8 eV and 286.6 eV assigned to carbon in the benzene and triazine ring can be clearly seen. The peak at 398.8 eV ascribed to N 1s nitrogen in the triazine ring appeared in both CTF-1 (Fig. 2c). Compared with AA stacking, AB stacking CTF-1 showed the residual nitrile monomers (400.1 eV) trapped in the interlayer and protonated nitrile groups (402.5 eV) (C = NH^+). As can be inferred from the XPS data of C 1s and N 1s, benzene and triazine rings survived in AA stacking CTF-1. The completion of the reaction and the stretching vibration of the framework through the formation of β-ketoenamine functionalities have been confirmed by Fourier transform infrared spectroscopy (FTIR) analysis [36]. Three new peaks at 800, 1349 and 1501 cm^{-1} assigned to the formation of triazine rings appeared in AB stacking CTF-1, it corresponded to the formation of triazine rings. After thermal treatment of AB stacking CTF-1 at 350 °C under nitrogen for 2 h, no changes were found in the FTIR spectrum of AA stacking (Fig. 2d), which demonstrate that the characteristic peaks for triazine units were well preserved during thermal treatment. Moreover, the FTIR data shows that the structure of CTF has not changed after illumination in Fig.S5. The TGA data reveals high thermal stability of the AA and AB CTF-1 with no decomposition up to ~400 °C (Fig. S6). The weight loss of both CTF-1 began at 650 °C, which may be caused by the decomposition of CTF-1 framework. Based on the above analysis, we confirmed that the AA and AB stacking CTF-1 were successfully synthesized. SEM and TEM images of AA and AB stacking CTF-1 showed nubbly morphologies of both CTF-1 (Fig. S7-8).

3.2. Photoelectric properties

The UV–vis diffuse reflectance spectroscopy (DRS) measurements were applied to study the light absorption ability of the CTF-1. Both samples display a wide range of light absorption (Fig. 3a), which could be attributed to faster intramolecular charge transfer from the donor to acceptor and more extended π-electron

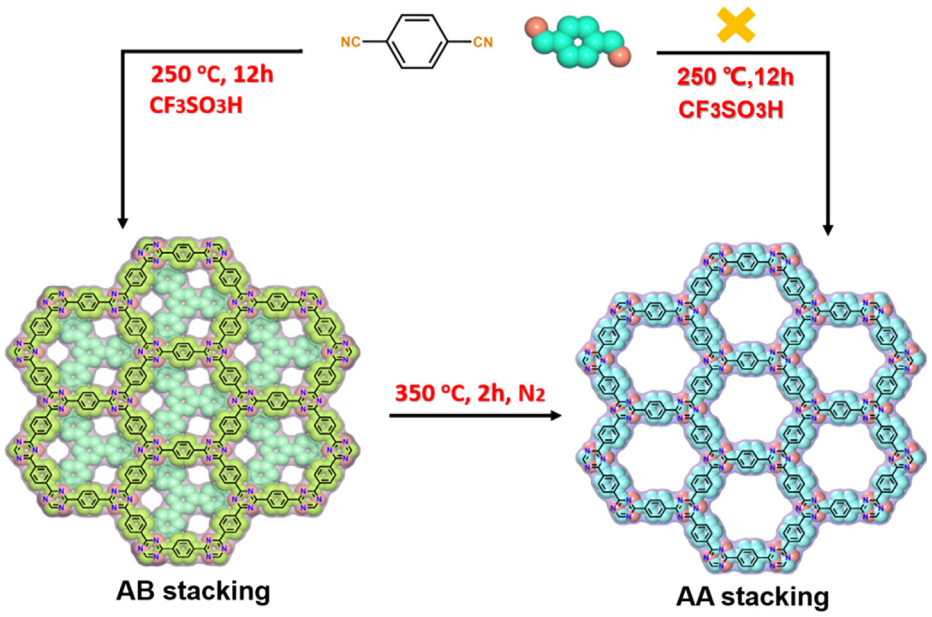

Scheme 1. Synthetic route of AA and AB stacking CTF-1 under mild conditions.

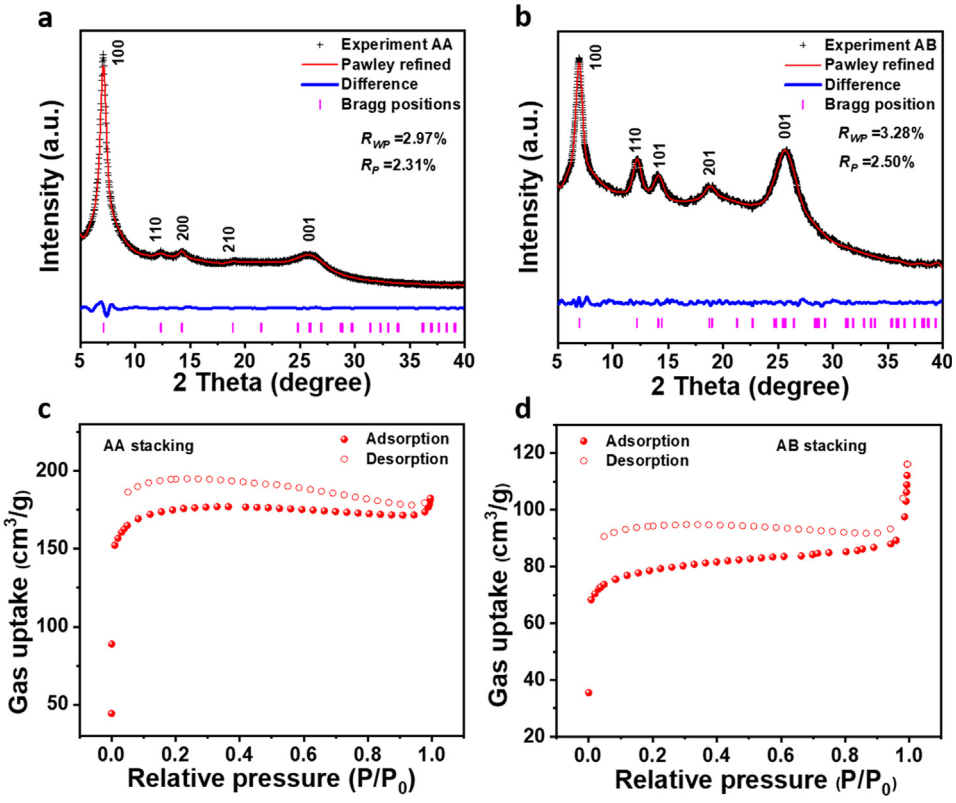

Fig. 1. Experimentally observed PXRD patterns (red cycle), Pawley-refined patterns (black line), the Bragg positions (pink line), and the difference between experimental and calculated data (blue line) of (a) AA stacking CTF-1 and (b) AB stacking CTF-1. (c) Nitrogen isotherms of AA stacking CTF-1. (d) Nitrogen isotherms of AB stacking CTF-1. (For interpretation of the references to colour in this figure legend, the reader is referred to the web version of this article.)

delocalization in CTF-1. On the basis of the Tauc plot (Fig. S9), the corresponding band gaps of AB stacking CTF-1 and AA stacking CTF-1 were calculated to be 2.52 eV and 2.13 eV, respectively. These results indicate that both CTF-1 possess the strong light absorption capacity. Moreover, the Mott-Schottky (M–S) measurements were employed to estimate the highest occupied molecular orbital (HOMO) and the lowest unoccupied molecular orbital (LUMO) levels. The positive slopes of two curves in the Fig. 3b confirm that these two CTF-1 are *n*-type semiconductors. Moreover, the flat band potential (V_{FB}) of AB stacking and AA stacking CTF-1 were calculated to be −0.72 V and −0.54 V vs normal hydrogen electrode (NHE). Based on the literature, the flat band potential is 0.1–0.3 V higher than their LUMO levels in an *n*-type semiconductor [33,37]. Therefore, the LUMO levels of AB and AA stacking CTF-1

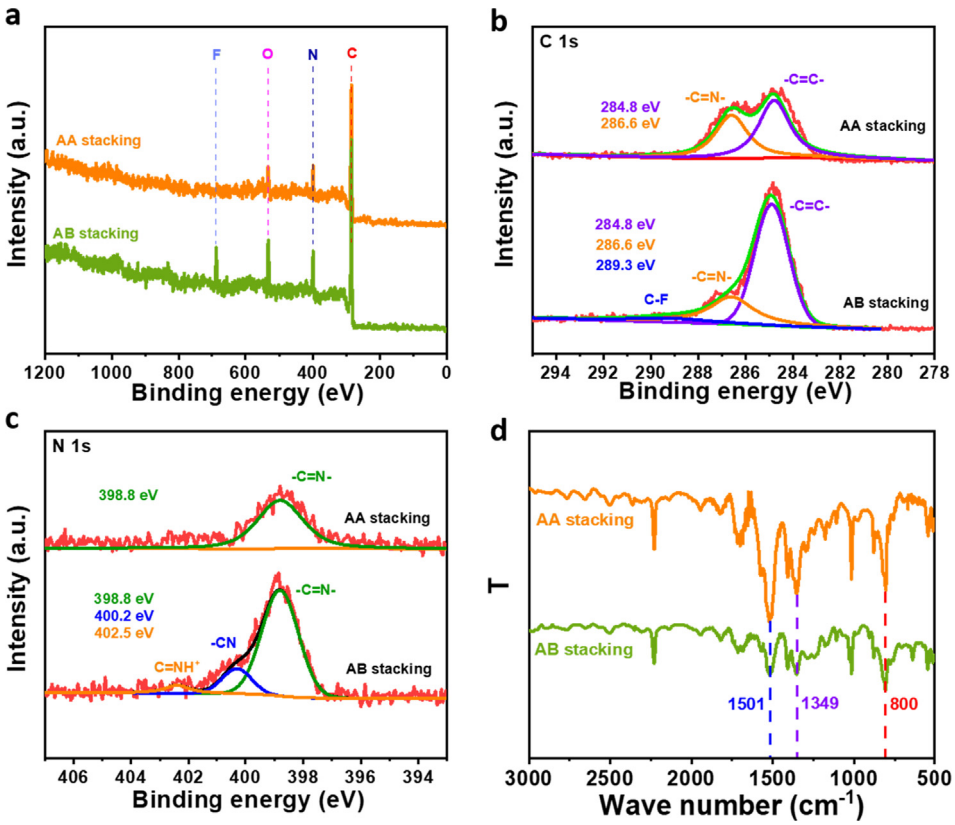

Fig. 2. (a) XPS survey curves of AA and AB stacking CTF-1, (b) XPS curves of the C 1s, (c) N 1s and (d) FT-IR spectra of AA and AB stacking CTF-1.

were estimated to −0.52 and −0.34 eV (vs. NHE), respectively. The higher-lying LUMO levels suggest that both CTF-1 are outstanding candidates for the transfer of photo-generated electrons for H_2 evolution. Moreover, combined with the bandgap from UV–vis absorption data, the HOMO levels were assessed to be 2.00 and 1.79 eV for AB and AA stacking CTF-1, respectively. Experimental data shows that AB stacking CTF-1 has a more optimized reduction potential to participate in the hydrogen evolution process (Fig. S10). We also applied the first-principles calculations through density functional theory (DFT). The density of states in Fig. 3c-d show that the energy gaps of AB and AA stacking CTF-1 were calculated to be approximately 2.1 and 1.8 eV, respectively. The variation tendency of the Eg from simulation was in accordance with that obtained from the experimental results. The steady-state photoluminescence (PL) spectra were performd to further investigate the photocatalytic properties of AA and AB stacking CTF-1. Theoretically, a low PL intensity indicates a low recombination efficiency of photogenerated electron hole pairs, thus resulting in a high photocatalytic performance [38]. In the present study, AB stacking CTF-1 exhibited a much lower photoluminescence than AA stacking CTF-1 at the same excitation wavelength of 375 nm (Fig. 3e), suggesting that the AB stacking CTF-1 possesses higher efficiency in charge separation than AA stacking CTF-1. In addition, the ESR of AB stacking and AA stacking CTF-1 was conducted to detect the defects and states of the materials with unpaired electrons. The ESR spectra displayed one single Lorentzian line centered at g value of 2.004 in dark (The g value was calculated using calculate in Supporting information) (Fig. 3f), which may be originated from unpaired electrons on π-conjugated aromatic rings of materials, demonstrating the existence of anion radical species. It was noted that the AB stacking CTF-1 showed much sharper EPR signal than AA stacking CTF-1, implying that AB stacking CTF-1 possesses the more anion radical species to participate in the H_2 evolution reaction of water.

3.3. Photocatalytic hydrogen evolution

Theoretically, CTF-1 possess delocalized π-bonds, which provide established pathways for charge carrier transport and lead to high efficiency for hydrogen evolution. More importantly, due to the higher electronegativity from N atoms and lower-energy π-orbital from C=N groups, the AB stacking CTF-1 exhibits a strong electron-withdrawing property [8,39]. Based on its highly porous geometrical energy minimization of AA and AB stacking CTF-1 from DFT calculation, layer-to-layer distance of eclipsed AA was estimated to about 3.434 Å whereas the staggered AB was about 7.010 Å. (Fig. 4) Herein, the H_2O could enter the inside of the CTF-1 although the pore size of the staggered AB stacking is relatively small. Thus, the layer-to-layer distance of AB stacking CTF-1 is more conducive to let H_2O molecules contact with exposed N atoms, which will facilitate the reduction of water. To verify the photocatalytic ability, we performed a continuous-flow system to monitor the H_2 evolution performance of the CTF-1. The photocatalytic H_2 production activity of both CTF-1 was examined under visible light (≥395 nm) in the presence of Pt cocatalyst by reducing the overpotential of proton reduction and TEOA as sacrificial electron donor to regenerate the photocatalyst through capturing the photogenerated holes. As we expected, AB stacking CTF-1 exhibited a high H_2 evolution rate with 362 μmol g^{-1} h^{-1} and the AA stacking CTF-1 showed a relatively low H_2 evolution rate with 70 μmol g^{-1} h^{-1} (Fig. 5a), which indicates that AB stacking CTF-1 has better photocatalytic reduction ability than AA stacking CTF-1. In addition, some high performance organic photocatalysts for H_2 evolution reaction under different light range irradiations have

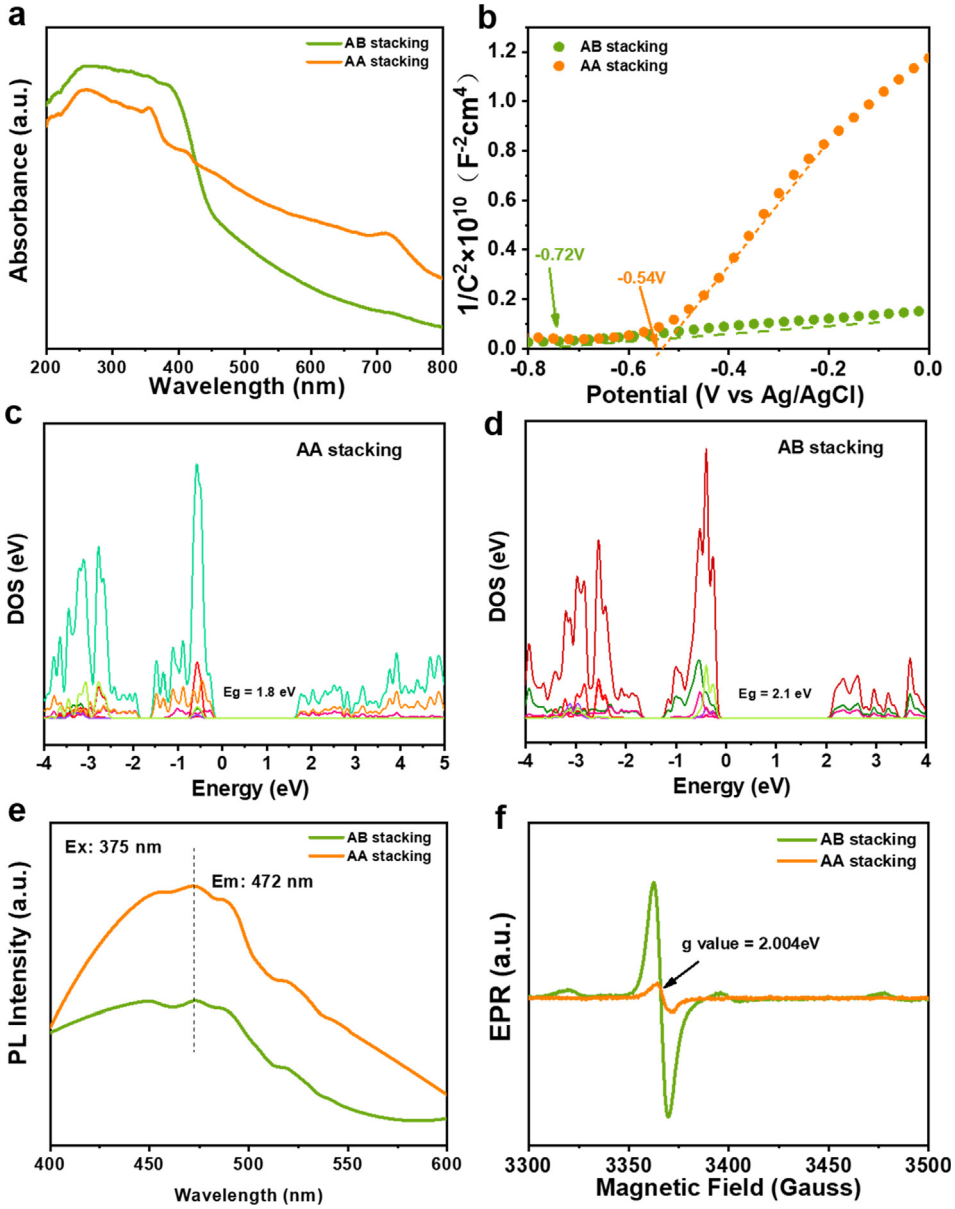

Fig. 3. (a) UV–vis absorption spectra of AA and AB stacking CTF-1. (b) Mott–Schottky plots for AA and AB stacking CTF-1. (c-d) Partial densities of AA and AB stacking states. (e) Photoluminescence (PL) emission spectra of AA and AB stacking CTF-1. (f) EPR spectra of AA and AB stacking CTF-1.

also summarized (Table S1). Compared with other COFs and CTFs catalysts, the AB stacking CTF-1 in this work showed excellent hydrogen production activity, which would bring organic catalysts to a new level in the field of photocatalysis. To further assure the superiority of the CTF-1 photocatalyst, the cycling performance of AA and AB stacking CTF-1 photocatalyst was evaluated for H_2 evolution as depicted in Fig. S11. The results showed that the CTF-1 photocatalyst possesses high durability for H_2 evolution by implying almost no photoactivity reduce after two cycles for 6 h continuous illumination. Moreover, the distinct photoelectric activity of the AA and AB stacking CTF-1 inspired us to further evaluate their PEC properties [40,41]. As shown in Fig. 5b, the cathodic photocurrent of AB stacking CTF-1 exhibited 77 μA cm^{-2} at 0 V vs. RHE based on the linear sweep voltammograms (LSV) in sodium sulfate electrolyte (0.5 M, pH 6.8) under air mass 1.5 global (AM 1.5G) light irradiation, it was nearly 2-fold higher than that of AA stacking CTF-1 (47 μA cm^{-2}). The LSV curves of these samples without AM 1.5G irradiation are shown in Fig. S12. The lower overpotential and sharp increase in photocurrent density of AB stacking CTF-1 demonstrate that the AB stacking possesses better photocatalytic performance than AA stacking. Besides, the results of transient photocurrent measurements in Fig. 5c show that the photocurrent of AB stacking CTF-1 is higher than that of AA stacking CTF-1 in several switch on–off cycles, it indicates that AB stacking also has better water oxidation ability than AA stacking. Meanwhile, the charge transfer resistance and separation ability of photogenerated carriers in two photocatalysts were further studied by the electrochemical impedance spectroscopy (EIS) measurement at 0 V vs. RHE. The smaller radius implies the smoother charge transfer [42,43]. As shown in Fig. 5d, the radius of semicircle for AB stacking CTF-1 decreased dramatically in comparison with AA stacking CTF-1, suggesting that the AB stacking CTF-1 could obviously enhance the charge transfer. These observations were consistent with the results of hydrogen evolution.

To acquire in-depth exploration of the charge transfer of AB, AA stacking CTF-1, the photophysical method (SPV and TPV) (introduction of instruments in supporting information) and theoretical calculations are implemented [44–46]. Traditionally, the positive

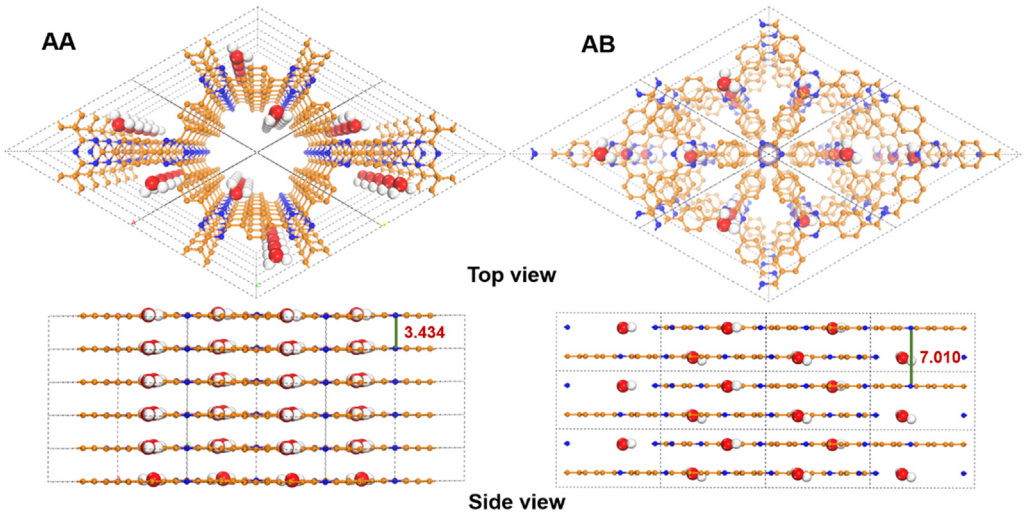

Fig. 4. DFT-optimized structures of the AA and AB stacking orders, together with their layer spacing.

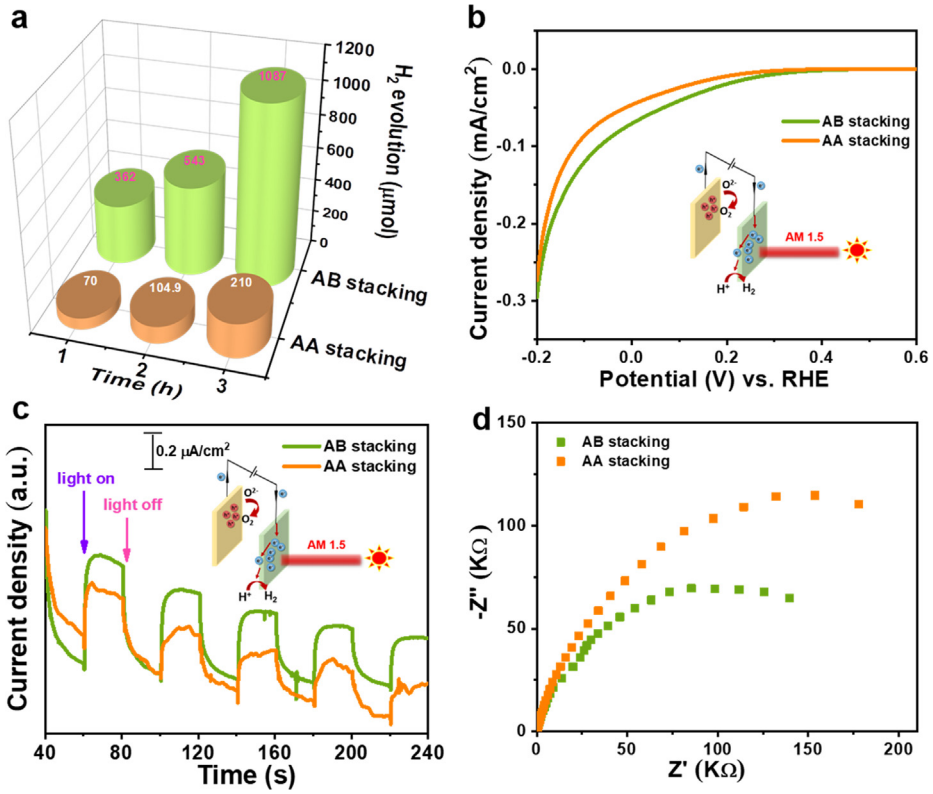

Fig. 5. (a) The photocatalytic H_2 evolution capacity of AA and AB stacking CTF-1. (b) LSV of AA and AB stacking CTF-1 under AM1.5 light irradiation in 0.5 M Na_2SO_4 electrolyte. (c) The i-t curve of AA and AB stacking CTF-1 under chopped light illumination at 1.23 V vs. RHE. (d) Impedance analyses for AA and AB stacking CTF-1 at 0 V vs. RHE.

signal represents that the holes transfer to the surface, whereas negative signal indicates that the migration of electrons to the surface. In this work, the SPV spectra of AB, AA stacking CTF-1 with front side illumination were investigated. As expected, both AB and AA stacking CTF-1 exhibited negative signals (Fig. S13), revealing that the photo-generated electrons transferred to the surface to participate in the reduction reaction of water. In addition, compared to AA stacking CTF-1, AB stacking CTF-1 presented increasing photovoltage intensity, suggesting the improved separation efficiency of AB stacking CTF-1. To further probe the dynamics of photogenerated charge carriers, the conventional TPV signal of CTF-1 under 532 nm laser pulse was recorded to evaluate the separation efficiency. The AB stacking CTF-1 displayed weaker positive signal than AA stacking CTF-1, manifesting that more electrons migrate to the surface to combine with holes (Fig. S14). The above analysis clearly proves that AB stacking CTF-1 possesses outstanding charge separation efficiency.

4. Conclusions

In summary, we designed and synthesized staggered crystalline AB stacking CTF-1 materials with more active sites under mild con-

ditions without the requirement of metal species or organic solvents. Unlike previous researches in which eclipsed AA stacking exhibited a better photocatalytic activity, in this work, remarkable enhancement in photocatalytic H_2 evolution was achieved in AB stacking CTF-1 in virtue of more active sites related to particular structures. The AB stacking CTF-1 exhibited outstanding photocatalytic H_2 evolution (362 μmol $g^{-1}h^{-1}$) under visible light, which was much higher than that of AA stacking CTF-1 (70 μmol h^{-1} g^{-1}), which may be attributed to more N atoms with higher electron-withdrawing effect involved in the water reduction reaction. Moreover, as the cathode material for PEC water reduction, AB stacking CTF-1 displayed an excellent saturated photocurrent density up to 77 μA cm^{-2} at 0 V vs. RHE, which is superior to the AA stacking CTF-1 (47 μA cm^{-2}). The present work would stimulate the future development of AB stacking CTFs in the field of photocatalysis.

CRediT authorship contribution statement

Yinyin Li: Conceptualization, Methodology, Validation, Investigation, Writing – original draft, Visualization. **Rui Zhang:** Investigation, Formal analysis. **Cuiyan Li:** Formal analysis, Software. **Hui Li:** Conceptualization, Funding acquisition, Supervision. **Qianrong Fang:** Conceptualization, Funding acquisition, Supervision. **Tengfeng Xie:** Conceptualization, Funding acquisition, Supervision.

Declaration of Competing Interest

The authors declare that they have no known competing financial interests or personal relationships that could have appeared to influence the work reported in this paper.

Acknowledgements

We are grateful to the National Natural Science Foundation of China (No. 21773086, 22025504, 21621001, and 21390394), ″111″ project (BP0719036 and B17020), and China Postdoctoral Science Foundation (2020TQ0118 and 2020M681034).

Appendix A. Supplementary material

Supplementary data to this article can be found online at https://doi.org/10.1016/j.jcis.2021.10.100.

References

[1] W. Jiang, D. Qu, L. An, X. Gao, Y. Wen, X. Wang, Z. Sun, J. Mater. Chem. A 7 (2019) 18348–18356.
[2] A. Fujishima, K. Honda, Nature 238 (1972) 37–38.
[3] J. Li, G. Zhan, Y. Yu, L. Zhang, Nat. Commun. 7 (2016) 11480.
[4] Y.-H. Yao, J. Li, H. Zhang, H.-L. Tang, L. Fang, G.-D. Niu, X.-J. Sun, F.-M. Zhang, J. Mater. Chem. A 8 (2020) 8949–8956.
[5] M. Bhadra, S. Kandambeth, M.K. Sahoo, M. Addicoat, E. Balaraman, R. Banerjee, J. Am. Chem. Soc. 141 (2019) 6152–6156.
[6] J. Shi, F. Chen, L. Hou, G. Li, Y. Li, X. Guan, H. Liu, L. Guo, Appl. Catal. B-Environ. 280 (2021).
[7] M. Liu, L.-Z. Qiao, B.-B. Dong, S. Guo, S. Yao, C. Li, Z.-M. Zhang, T.-B. Lu, Appl. Catal. B-Environ. 273 (2020) 119066.
[8] Z. Zhao, Y. Zheng, C. Wang, S. Zhang, J. Song, Y. Li, S. Ma, P. Cheng, Z. Zhang, Y. Chen, ACS Catal. 11 (2021) 2098–2107.
[9] S. Ghosh, A. Nakada, M.A. Springer, T. Kawaguchi, K. Suzuki, H. Kaji, I. Baburin, A. Kuc, T. Heine, H. Suzuki, R. Abe, S. Seki, J. Am. Chem. Soc. 142 (2020) 9752–9762.
[10] T. Banerjee, K. Gottschling, G. Savasci, C. Ochsenfeld, B.V. Lotsch, ACS Energy Lett. 3 (2018) 400–409.
[11] B.P. Biswal, H.A. Vignolo-Gonzalez, T. Banerjee, L. Grunenberg, G. Savasci, K. Gottschling, J. Nuss, C. Ochsenfeld, B.V. Lotsch, J. Am. Chem. Soc. 141 (2019) 11082–11092.
[12] X. Wang, L. Chen, S.Y. Chong, M.A. Little, Y. Wu, W.H. Zhu, R. Clowes, Y. Yan, M. A. Zwijnenburg, R.S. Sprick, A.I. Cooper, Nat. Chem. 10 (2018) 1180–1189.
[13] W. Li, X. Huang, T. Zeng, Y.A. Liu, W. Hu, H. Yang, Y.B. Zhang, K. Wen, Angew. Chem. Int. Ed. 60 (2021) 1869–1874.
[14] X. Wang, K. Maeda, A. Thomas, K. Takanabe, G. Xin, J.M. Carlsson, K. Domen, M. Antonietti, A metal-free polymeric photocatalyst for hydrogen production from water under visible light, Nat. Mater. 8 (2009) 76–80.
[15] X. He, H. Fang, D.J. Gosztola, Z. Jiang, P. Jena, W.N. Wang, ACS Appl. Mater. Interfaces 11 (2019) 12516–12524.
[16] C. Chen, A. Wu, H. Yan, Y. Xiao, C. Tian, H. Fu, Chem. Sci. 9 (2018) 4746–4755.
[17] L. Wang, Y. Zhang, L. Chen, H. Xu, Y. Xiong, Adv. Mater. 30 (2018) 1801955.
[18] L. Li, W. Fang, P. Zhang, J. Bi, Y. He, J. Wang, W. Su, J. Mater. Chem. A 4 (2016) 12402–12406.
[19] X. Jiang, P. Wang, J. Zhao, J. Mater. Chem. A 3 (2015) 7750–7758.
[20] L. Stegbauer, S. Zech, G. Savasci, T. Banerjee, F. Podjaski, K. Schwinghammer, C. Ochsenfeld, B.V. Lotsch, Adv. Energy Mater. 8 (2018) 1703278.
[21] T. Sick, A.G. Hufnagel, J. Kampmann, I. Kondofersky, M. Calik, J.M. Rotter, A. Evans, M. Doblinger, S. Herbert, K. Peters, D. Bohm, P. Knochel, D.D. Medina, D. Fattakhova-Rohlfing, T. Bein, J. Am. Chem. Soc. 140 (2018) 2085–2092.
[22] V.S. Vyas, F. Haase, L. Stegbauer, G. Savasci, F. Podjaski, C. Ochsenfeld, B.V. Lotsch, Nat. Commun. 6 (2015) 8508.
[23] C.B. Meier, R.S. Sprick, A. Monti, P. Guiglion, J.-S.-M. Lee, M.A. Zwijnenburg, A.I. Cooper, Polymer 126 (2017) 283–290.
[24] W. Huang, J. Byun, I. Rorich, C. Ramanan, P.W.M. Blom, H. Lu, D. Wang, L. Caire da Silva, R. Li, L. Wang, K. Landfester, K.A.I. Zhang, Angew. Chem. Int. Ed. 57 (2018) 8316–8320.
[25] S. Zhang, G. Cheng, L. Guo, N. Wang, B. Tan, S. Jin, Angew. Chem. Int. Ed. 59 (2020) 6007–6014.
[26] Q. Jiang, L. Sun, J. Bi, S. Liang, L. Li, Y. Yu, L. Wu, ChemSusChem 11 (2018) 1108–1113.
[27] M. Wei, W. Zhou, F. Xu, Y. Wang, Small 16 (2019) 1903879.
[28] D. Kong, X. Han, J. Xie, Q. Ruan, C.D. Windle, S. Gadipelli, K. Shen, Z. Bai, Z. Guo, J. Tang, ACS Catal. 9 (2019) 7697–7707.
[29] P. Kuhn, M. Antonietti, A. Thomas, Angew. Chem. Int. Ed. 47 (2008) 3450–3453.
[30] M. Liu, L. Guo, S. Jin, B. Tan, J. Mater. Chem. A 7 (2019) 5153–5172.
[31] Z. Yang, H. Chen, S. Wang, W. Guo, T. Wang, X. Suo, D.E. Jiang, X. Zhu, I. Popovs, S. Dai, J. Am. Chem. Soc. 142 (2020) 6856–6860.
[32] T. Jiang, T. Xie, W. Yang, L. Chen, H. Fan, D. Wang, J. Phys, Chem. C 117 (2013) 4619–4624.
[33] M. Zhang, M. Lu, Z.L. Lang, J. Liu, M. Liu, J.N. Chang, L.Y. Li, L.J. Shang, M. Wang, S.L. Li, Y.Q. Lan, Angew. Chem. Int. Ed. 59 (2020) 6500–6506.
[34] R. Zhang, L. Bi, D. Wang, Y. Lin, X. Zou, T. Xie, Z. Li, J. Colloid Interface Sci. 578 (2020) 431–440.
[35] S. Kuecken, A. Acharjya, L. Zhi, M. Schwarze, R. Schomacker, A. Thomas, Chem. Commun. 53 (2017) 5854–5857.
[36] D. Begue, G.G. Qiao, C. Wentrup, J. Am. Chem. Soc. 134 (2012) 5339–5350.
[37] Y. Sun, Q. Zhu, B. Bai, Y. Li, C. He, Chem. Eng. J. 390 (2020) 124518.
[38] L. Bi, X. Gao, L. Zhang, D. Wang, X. Zou, T. Xie, ChemSusChem 11 (2018) 276–284.
[39] J.W. Jung, F. Liu, T.P. Russell, W.H. Jo, Adv. Mater. 27 (2015) 7462–7468.
[40] H. Sun, C. Neumann, T. Zhang, M. Loffler, A. Wolf, Y. Hou, A. Turchanin, J. Zhang, X. Feng, Adv. Mater. 31 (2019) 1900961.
[41] S.-S. Yi, B.-R. Wulan, J.-M. Yan, Q. Jiang, Adv. Funct. Mater. 29 (2019) 1801902.
[42] Q. Bu, S. Li, Q. Wu, L. Bi, Y. Lin, D. Wang, X. Zou, T. Xie, ChemSusChem 11 (2018) 3486–3494.
[43] Y. Li, Q. Wu, Y. Chen, R. Zhang, C. Li, K. Zhang, M. Li, Y. Lin, D. Wang, X. Zou, T. Xie, Appl. Catal. B-Environ. 290 (2021) 120058.
[44] T. Jiang, T. Xie, L. Chen, Z. Fu, D. Wang, Nanoscale 5 (2013) 2938–2944.
[45] L. Bi, R. Zhang, K. Zhang, Y. Lin, D. Wang, X. Zou, T. Xie, ACS Sustain. Chem. Eng. 7 (2019) 15137–15145.
[46] Q. Qiu, S. Li, J. Jiang, D. Wang, Y. Lin, T. Xie, J. Phys. Chem. C 121 (2017) 21560–21570.